Journal of Textiles and Polymers
Vol. 11, No. 3, 49-57, June 2023
https://www.itast.ir
DOI: 10.48302/jtp.2024.481449.1299

Modeling Poisson's Ratio and Tensile Behavior of Auxetic 4-Plied Yarn

Milad Razbin*[1], Mortaza Salehian[2]

[1] Department of Textile Engineering, Amirkabir University of Technology, Tehran, Iran.
[2] Department of Aerospace Engineering, Amirkabir University of Technology, Tehran, Iran.

Article Information

Article history:

Received: 2024-10-02

Accepted: 2024-12-15

***Keywords*:**
Auxetic yarn,
Geometrical Modeling,
Mechanical Modeling,
Tensile Behavior,
Poisson's Ratio.

Abstract

Auxetic yarns, renowned for their unique capability to expand laterally when subjected to tensile loading, are gaining recognition as innovative and adaptable structural materials. These yarns hold significant promise across a wide range of applications, including the development of auxetic fabrics with enhanced properties, the reinforcement of composite materials for improved strength and durability, and the creation of advanced smart wearable sensors with heightened sensitivity and functionality. In this study, a comprehensive theoretical framework is introduced, consisting of a geometrical model to predict Poisson's ratio and a mechanical model aimed at forecasting the stress-strain behavior of auxetic 4-plied yarns (A4PY). The proposed models integrate key parameters, such as the radius of the components, their respective Young's modulus and Poisson's ratio, and the twist per meter of the yarn structure. Rigorous validation against experimental data from previously published studies confirms the accuracy and reliability of these models in capturing both the Poisson's ratio and the stress-strain responses, aligning with observed experimental trends.

1 INTRODUCTION

An auxetic is an object that widens when stretched and narrows when compressed. The term "auxetic metamaterials" refers to structural materials composed of soft and stiff segments, exhibiting negative Poisson's ratio with enhanced physicomechanical properties such as shear and fracture resistance, synclastic behavior, variable permeability, and energy absorption [1]. These metamaterials are classified into four primary groups including cellular, natural, metallic, and multi-material composites. They show promises for various applications including sensors, sports science, textiles, medicine, and defense [2]. Textiles form a category of multi-material composites that can be tailored in properties due to their diverse materials and structural geometries, available in forms like fibers, fibrous structures, yarns, and fabrics.

Various manufacturing methods have been explored to create auxetic textiles, particularly auxetic yarns, which have gained attention for their simple production and customizable properties. Hook *et al.* pioneered the helical auxetic yarn (HAY), featuring a high-diameter, low-modulus filament yarn as the core and a high-modulus, low-diameter yarn as the wrap, enhancing diameter under uniaxial tensile load [3]. Continued research has focused on optimizing HAY's mechanical properties and understanding the influences on its auxetic performance. Innovations in HAY design have included using additional wrap components or matrices to enhance structural stability and auxetic behavior [4, 5]. Theoretical studies have also developed models using analytical [6-9], numerical [10, 11], artificial neural network (ANN) [9], and statistical [12] approaches to predict the behavior of HAY. Zhang *et al.* modified the HAY structure by integrating a third component as a matrix to enhance its structural stability under various conditions [13]. Liu *et al.* proposed a variation of the HAY structure, incorporating an extra wrap component to increase cohesion and structural stability, resulting in superior auxetic performance compared to traditional HAY [8]. Shen and Adanur introduced a braided auxetic yarn design, noting a decrease in open area under tensile stress due to its unique auxetic properties, supported by multi-scale finite element analysis [14]. Lolaki *et al.* improved the auxetic performance of HAY using a multifilament wrap component and explored the differences between instantaneous and engineering Poisson's ratios to understand HAY's strain-dependent behavior, achieving notable auxetic results [15]. Razbin and Bagherzadeh proposed a model based on elasticity to predict the longitudinal young's modulus of helical auxetic yarn reinforced unidirectional composite [16]. Despite various reports on HAY's applications, Lim proposed a semi-auxetic yarn design that only exhibits auxetic behavior along one plane, utilizing a unique sewing pattern with an elastic and rigid cord [17]. Ge *et al.* developed an auxetic 4-plied yarn (A4PY) that alternates between high and low modulus monofilament yarns, which adjust under load to enhance its diameter [18]. Zeng and Hu further modified this model, providing better predictions of A4PY's behavior in early stages of loading through the introduction of a 'tilt angle' concept

*Corresponding Author: Milad.razbin@aut.ac.ir

[19]. Following this, Jiang and Hu designed braided auxetic yarn with enhanced structural stability and auxetic properties, confirmed by experimental data comparing theoretical models and actual performance [20]. Razbin *et al*. used an extra core yarn to increase structural stability and achieve a lower negative Poisson's ratio. They proposed analytical and ANN based models to predict the Poisson' ratio of yarn [21, 22]. Recent publications have highlighted the use of auxetic yarns as promising components in the creation of auxetic textile sensors [23-25]. It is anticipated that deeper theoretical analysis of the deformation behavior of auxetic yarns will provide valuable insights for researchers in their future applications.

This study focuses on A4PY due to its distinct structure compared to other auxetic yarns, which positions it as a potential candidate for smart textiles. Therefore, a thorough understanding of its deformation and tensile properties is essential. To date, there are few research papers that explore the structure of A4PY. Two theoretical models have been developed to estimate Poisson's ratio, both of which rely on a limited set of equations and numerical estimation. In this paper, we introduce a fully deterministic model designed to predict not only the Poisson's ratio but also the tensile behavior of the yarn. Experimental data from prior research is utilized to validate the proposed models.

2 MODELING

2-1 Structure, unit cell and assumptions

To initiate the modeling of the deformation behavior of Auxetic 4-plied Yarns (A4PY), a unit cell as depicted in Figure 1 has been chosen, representing a complete twist of the structure. The basic assumptions are:

- The cross-sections of both the soft and stiff yarns are assumed to be circular and to maintain their shape consistently until the culmination of the tensile loading.
- The model simplifies the interaction between components by assuming the absence of friction and indentation.
- The mechanical properties, including the Poisson's ratio and elastic behavior of the components, are presumed to remain constant throughout the entire duration of tensile loading.

This assumption facilitates a clearer understanding of the yarn's behavior under uniform stress conditions, providing a foundational model for further detailed analyses.

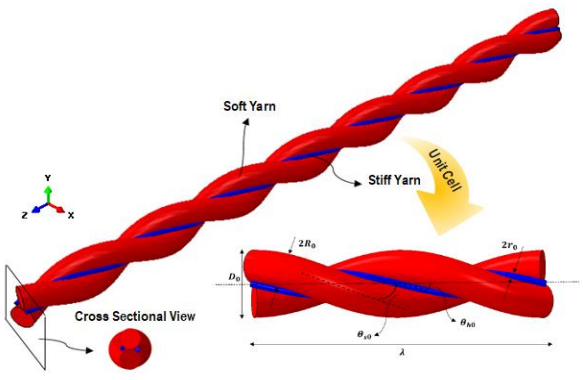

Fig. 1 Schematic illustration of A4PY structure and unit cell

Based on the geometry of the unit cell, the deformation behavior of structure could be shown in two directions including cross-sectional and longitudinal views as Figure 2 and Figure 3, respectively. It should be noted that the "X" and "Y" directions have considered showing the radial displacements of A4PY. At the initial state of the structure, the soft yarns are touching each other at the center point of the structure while the stiff yarns have been positioned in the side space of soft yarns (Figure 2a-Figure 3a). When the structure has been subjected to tensile loading, the stiff yarns start to move toward the center of the structure and push away the soft yarns. During this stage of loading, which is considered the first stage, the stiff yarns only displace but the soft yarns deform in addition to displacement (Figure 2b-Figure 3b). The condition of structure that stiff yarns touch each other has been considered as "jamming state" and it is a criterion that separates the first stage and second stage of the loading process (Figure 2b-Figure 3b). By applying more loading, the structure will undergo a second stage in which both components deform while keeping their position unchanged (Figure 2c-Figure 3c).

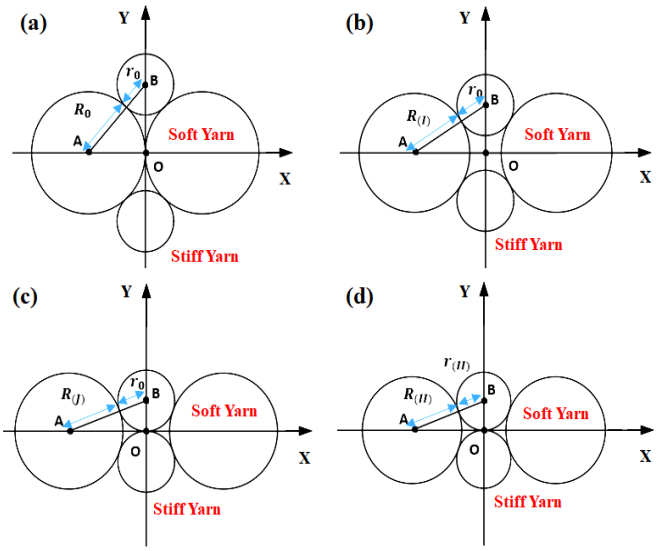

Fig. 2 Cross-sectional view of A4PY under tensile loading conditions: (a) initial state, (b) first stage, (c) jamming state, (d) second stage

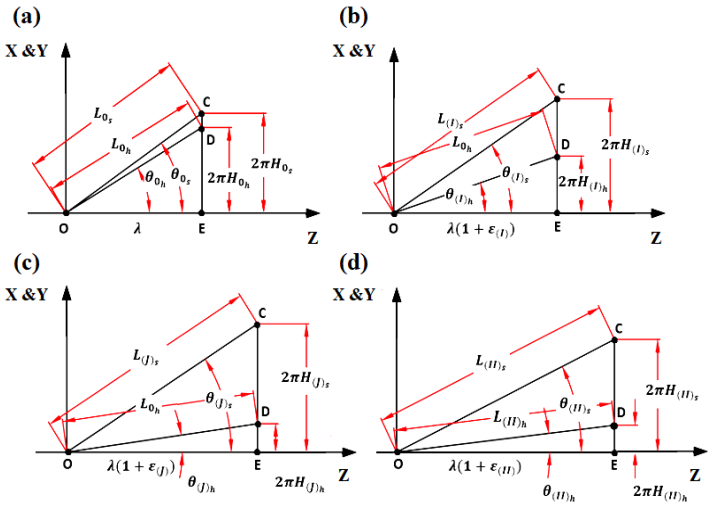

Fig. 3 Longitudinal view of A4PY under tensile loading conditions: (a) initial state, (b) first stage, (c) jamming state, (d) second stage

2-2 Geometrical analysis

2-2-1 Determination of initial structural parameters

According to Figure 3a, the initial structural parameters, including the pitch length (λ), helical radius of components (H), helical angle of components (θ), length of components per twist of structure (L), and the maximum diameter of the structure (D), can be calculated using the following equations. The input parameters for these equations are the radius of the components (R) and the twists per meter of the structure (TPM).

$$\lambda = \frac{1000}{TPM_{(i)}} \tag{1}$$

$$H_{s_{(i)}} = R_{s_{(i)}} \tag{2}$$

$$H_{h_{(i)}} = \sqrt{(R_{s_{(i)}} + R_{h_{(i)}})^2 - {R_{s_{(i)}}}^2} \tag{3}$$

$$\theta_{s_{(i)}} = \left(\frac{2\pi R_{s_{(i)}}}{\lambda}\right) \tag{4}$$

$$\theta_{h_{(i)}} = \left(\frac{2\pi\sqrt{(R_{s_{(i)}} + R_{h_{(i)}})^2 - {R_{s_{(i)}}}^2}}{\lambda}\right) \tag{5}$$

$$L_{s_{(i)}} = \sqrt{\lambda^2 + 4\pi^2 {R_{s_{(i)}}}^2} \tag{6}$$

$$L_{h_{(i)}} = \sqrt{\lambda^2 + 4\pi^2((R_{s_{(i)}} + R_{h_{(i)}})^2 - {R_{s_{(i)}}}^2)} \tag{7}$$

$$D_{(i)} = 4R_{s_{(i)}} \tag{8}$$

Where the indices i, s, and h refer to the initial state, soft yarn, and stiff yarn, respectively. Moreover, it is assumed that to achieve an auxetic effect in A4PY, the following criteria must be considered during production.

$$H_{h_{(i)}} + R_{h_{(i)}} < H_{s_{(j)}} + R_{s_{(j)}}$$

2-2-2 Determination of jamming strain

As mentioned above, the jamming strain divides the entire tensile process into two stages. To calculate the jamming strain, the following equation can be derived from Figure 3c: Table 1 C-Glass fiber and Epoxy resin properties

$$\varepsilon_{(j)} = \frac{\sqrt{{L_{h_{(i)}}}^2 - \left(2\pi R_{h_{(i)}}\right)^2}}{\lambda} - 1 \tag{9}$$

In general, Poisson's ratio of the structure can be expressed using Equation (10). To calculate it, the structure will be subjected to a specific amount of axial strain. Then, based on the variation in the structure's geometry, the corresponding maximum diameter (D) will be calculated.

$$\nu = -\frac{\varepsilon_D}{\varepsilon_L} = -\frac{D - D_{(i)}}{D_{(i)}\varepsilon} \tag{10}$$

$$D = 2(R_s + H_s) \tag{11}$$

2-2-3 Determination of Poisson's ratio in different stages

Based on the assumptions, stiff yarns are rigid during the first stage. Due to this assumption, the helical angle of the stiff yarn can be calculated using Equation (12).

$$\theta_{h_{(I)}} = \left(\left(1 + \varepsilon_{(I)}\right)\right) \tag{12}$$

Thus, the corresponding helical radius of the stiff yarn is also calculable.

$$H_{h_{(I)}} = \frac{L_{h_{(i)}}\, sin\, sin\left(\theta_{h_{(I)}}\right)}{2\pi} \tag{13}$$

Based on Figure 3b, the following relationship has been established between the helical radius and the radius of the components:

$${H_{s_{(I)}}}^2 = \left(R_s + R_{h_{(i)}}\right)^2 - {H_{h_{(I)}}}^2 \tag{14}$$

In addition, the corresponding radius of the soft yarn follows Equation (15):

$$R_s = R_{s_{(i)}}\left(1 - \nu_s \frac{L_{s_{(I)}} - L_{s_{(i)}}}{L_{s_{(i)}}}\right) \tag{15}$$

According to the position of the soft yarn, the following equation can be used to express its length during the tensile loading:

$${L_{s_{(I)}}}^2 = \left(2\pi H_{s_{(I)}}\right)^2 + \lambda^2\left(1 + \varepsilon_{(I)}\right)^2 \tag{16}$$

By substituting Equations (10) through (13) into Equation (14), we obtain

$${L_{s_{(I)}}}^2 = 4\pi^2\Bigg(\left(R_{s_{(i)}}\left(1 - \nu_s \frac{L_{s_{(I)}} - L_{s_{(i)}}}{L_{s_{(i)}}}\right) + R_{h_{(i)}}\right)^2 - {H_{h_{(I)}}}^2\Bigg) + \lambda^2\left(1 + \varepsilon_{(I)}\right)^2 \tag{17}$$

By solving Equation (17) under various amounts of axial strain according to input parameters, the corresponding lengths of the soft yarn, as well as the corresponding radii and helical radii of the soft yarns, can be calculated. It should be noted that the strain applied to the structure during the first stage must adhere to the following criteria:

$$0 \le \varepsilon_{(I)} \le \varepsilon_{(j)}$$

In the second stage of the tensile process, the stiff yarn also begins to deform. In the first step of the calculation, based on the geometry of the structure, the following equation can be used to express the length of the stiff yarn during the second stage of loading.

$${L_{h_{(II)}}}^2 = \left(2\pi R_{h_{(II)}}\right)^2 + \lambda^2\left(1 + \varepsilon_{(II)}\right)^2 \tag{18}$$

In addition, the corresponding radius of the stiff yarn follows the equation below

$$R_{h_{(II)}} = R_{h_{(i)}}\left(1 - \nu_h \frac{L_{h_{(II)}} - L_{h_{(i)}}}{L_{h_{(i)}}}\right) \tag{19}$$

By substituting Equation (17) into Equation (16), we obtain:

$$L_{h_{(II)}}{}^2 = \left(2\pi R_{h_{(i)}}\left(1 - \nu_h \frac{L_{h_{(II)}} - L_{h_{(i)}}}{L_{h_{(i)}}}\right)\right)^2 + \lambda^2\left(1 + \varepsilon_{(II)}\right)^2 \quad (20)$$

In the second step of the calculation, the same approach that was used in the first stage to calculate the length of the soft yarn will be employed, but this time the deformation of the stiff yarns will also be considered.

$$L_{s_{(II)}}{}^2 = 4\pi^2\left(\left(R_{s_{(i)}}\left(1 - \nu_s \frac{L_{s_{(II)}} - L_{s_{(i)}}}{L_{s_{(i)}}}\right) + R_{h_{(II)}}\right)^2 - R_{h_{(II)}}{}^2\right) + \lambda^2\left(1 + \varepsilon_{(II)}\right)^2 \quad (21)$$

The applied strain on the structure during the second stage of loading must adhere to the following criteria

$$\varepsilon_{(j)} \leq \varepsilon_{(II)} \leq \varepsilon_{rup}$$

During the calculation, the indices I and II refer to the first stage and second stage of the loading process, respectively. The flowchart to calculate Poisson's ratio-strain is presented in Figure 4.

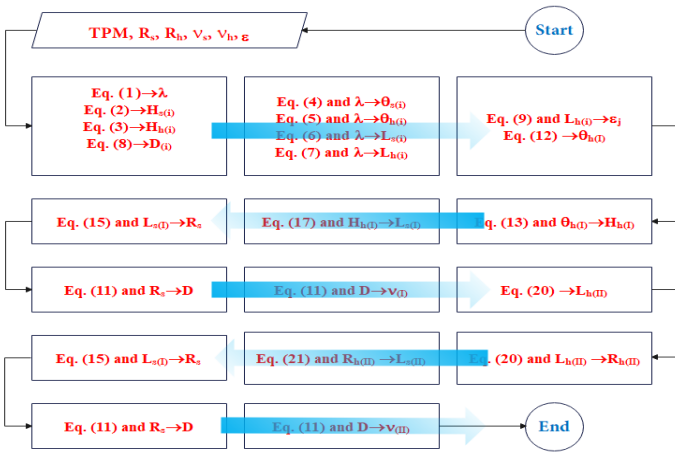

Fig. 4 Flowchart for calculation of Poisson's ratio-strain curve for A4PY

2-3 Mechanical analysis

In this section, a geometrical model is used to calculate the force acting on the filaments. Using the elastic behavior of materials, the stress applied to the structure can be calculated using Equation (22).

$$\sigma_y = \frac{F_y}{2A_{s(i)} + 2A_{h(i)}} \quad (22)$$

In which

$$A_{s(i)} = \pi R_{s_{(i)}}{}^2 \quad (23)$$

$$A_{h(i)} = \pi R_{h_{(i)}}{}^2 \quad (24)$$

When A4PY is subjected to axial tensile loading, the total force acting on the structure is the sum of the forces acting on the components, which include two soft monofilament yarns and two stiff monofilament yarns. In other words:

$$F_y = \frac{2F_h}{cos(\theta_h)} + \frac{2F_s}{cos(\theta_s)} \quad (25)$$

Where F_h and F_s represent the axial forces acting on the stiff and soft monofilament yarns, respectively. Given the assumption that stiff monofilaments do not undergo deformation in the first stage of loading, Equation (22) can be rewritten as follows.

$$F_{y_{(I)}} = \frac{2F_s}{cos(\theta_{s_{(I)}})} \quad (26)$$

In the following, the total force acting on A4PY in the second stage of loading can be calculated using Equation (27).

$$F_{y_{(II)}} = \frac{2F_h}{cos(\theta_{h_{(II)}})} + \frac{2F_s}{cos(\theta_{s_{(II)}})} \quad (27)$$

To estimate the force acting on the monofilaments either in first or second stages, Equation (28) can be expressed according to Hooke's law as follows:

$$F_{h.s} = (EA\varepsilon)_{h.s} \quad (28)$$

It should be noted that during the calculations using the proposed model, Poisson's ratio of components can be formulated as a polynomial function to obtain precise results, as demonstrated in previous works [7, 8]. The same approach can be applied to Young's modulus of the components. However, neither of these aspects is addressed in this work due to limited access to experimental data. The flowchart to calculate stress-strain is presented in Figure 5.

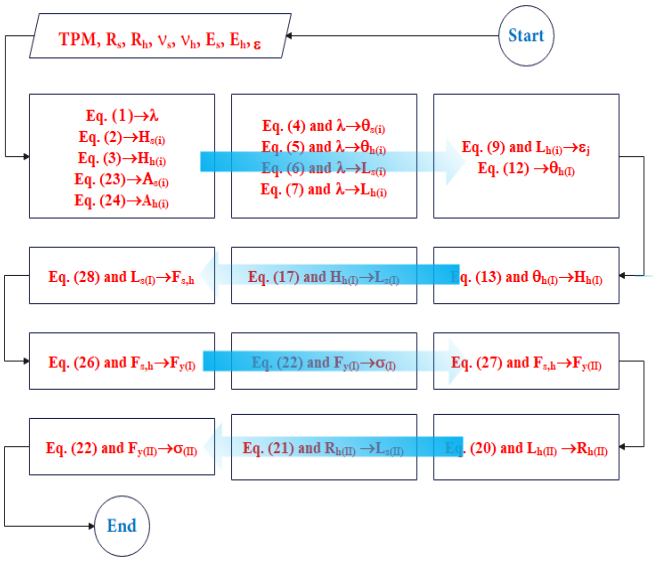

Fig. 5 Flowchart for calculation of stress-strain curve for A4PY

3 RESULTS and DISCUSSIONS

To confirm the accuracy of the proposed model, we utilized data from prior research [18, 19, 26, 27]. Table 1 presents a summary of the input parameter values derived from various studies. A total of 12 samples were analyzed to validate the proposed model.

Table 1 Input parameters of the model

Ref.	Sample code	TPM (turn/m)	R_s (mm)	E_s (MPa)	ν_s	R_h (mm)	E_h (MPa)	ν_h
[18]	E1	52.63	1.02	4.49	0.30	0.39	1017.15	0.30
	E2	53.33	1.02	4.49	0.30	0.09	4178.07	0.30
	E3	50.71	0.51	1.56	0.30	0.39	1017.15	0.30
	E4	89.73	0.51	1.56	0.30	0.09	4178.07	0.30
[19]	E5	51.02	1.09	13.00	0.15	0.385	1300.00	0.30
[26]	E6	51.02	1.09	13.00	0.15	0.385	1300.00	0.15
[27]	E7	51.00	1.09	13.00	0.15	0.435	630.00	0.15
	E8	51.00	1.09	13.00	0.15	0.385	1307.00	0.15
	E9	51.00	0.57	8.00	0.15	0.435	630.00	0.15
	E10	51.00	0.57	8.00	0.15	0.385	1307.00	0.15
	E11	35.00	1.09	13.00	0.15	0.435	630.00	0.15
	E12	65.00	1.09	13.00	0.15	0.435	630.00	0.15

3-1 Validation of models

In this work, models for predicting Poisson's ratio-strain and stress-strain curves of A4PY are presented. Figure 6 illustrates a comparison between the experimental results and the predictions made by the proposed model for Poisson's ratio-strain curve. For samples E1-E4, the proposed model demonstrates a trend that aligns closely with the experimental results, capturing the overall behavior of the material under tensile loading. However, some discrepancies are observed during the initial stages of the tensile process. These discrepancies can be attributed to challenges in accurately measuring Poisson's ratio at low strain levels. Specifically, before the application of load, structural gaps within the samples lead to measurement inconsistencies. For samples E5 and E6, the differences between experimental and predicted values are more pronounced, particularly in the mid-strain regions. These deviations highlight the complexities involved in modelling the intricate interactions within the material structure under tensile strain. The correlation between the experimental and predicted data remains significant, but the observed deviations underscore the need for further refinement in the modelling of specific structural parameters such as indentation effect. In samples E7-E12, the primary differences between the experimental and predicted data occur in the strain region before the jamming strain. These differences are likely influenced by structural instabilities and measurement errors that arise during the early stages of deformation. Despite these deviations, the proposed model successfully captures the impact of critical structural parameters, such as twisting angles and component diameters, on Poisson's ratio-strain relationship. The results indicate that the proposed model provides a robust framework for understanding the deformation behavior of A4PY, even though certain limitations remain in accurately representing low-strain behaviors.

Figure 7 presents the comparison between the experimental results and the predictions made by the proposed model for the stress-strain behavior of samples E7-E12. The model effectively captures the general bi-linear trend observed in the experimental data, particularly in the pre-jamming strain regions. However, notable discrepancies arise in the regions beyond the jamming strain. These differences are attributed to the assumption of linear behavior for both the soft and stiff yarns in the proposed model, which does not fully capture the nonlinear mechanical interactions occurring in the post-jamming regime.

The mechanical proposed model is designed to predict the stress-strain behavior of A4PY by incorporating linear assumptions for its components. While this approach enables the model to represent the tensile response through a bi-linear methodology, it simplifies the material's behavior, particularly the stiff yarn's response. This simplification leads to inaccuracies in stress-strain predictions under high-strain conditions. Despite these limitations, the model demonstrates the excellent potential to account for variations in mechanical behavior across different samples, highlighting its adaptability. To enhance the accuracy of predictions, it is recommended to replace the linear assumption with a nonlinear function that better represents the tensile behavior of the individual components. By incorporating a variable Young's modulus or a more complex constitutive relation, the model could provide a more realistic representation of the material's mechanical properties, particularly in the post-jamming regions. This adjustment would allow the model to reflect the actual behavior of the material under varying conditions with greater precision.

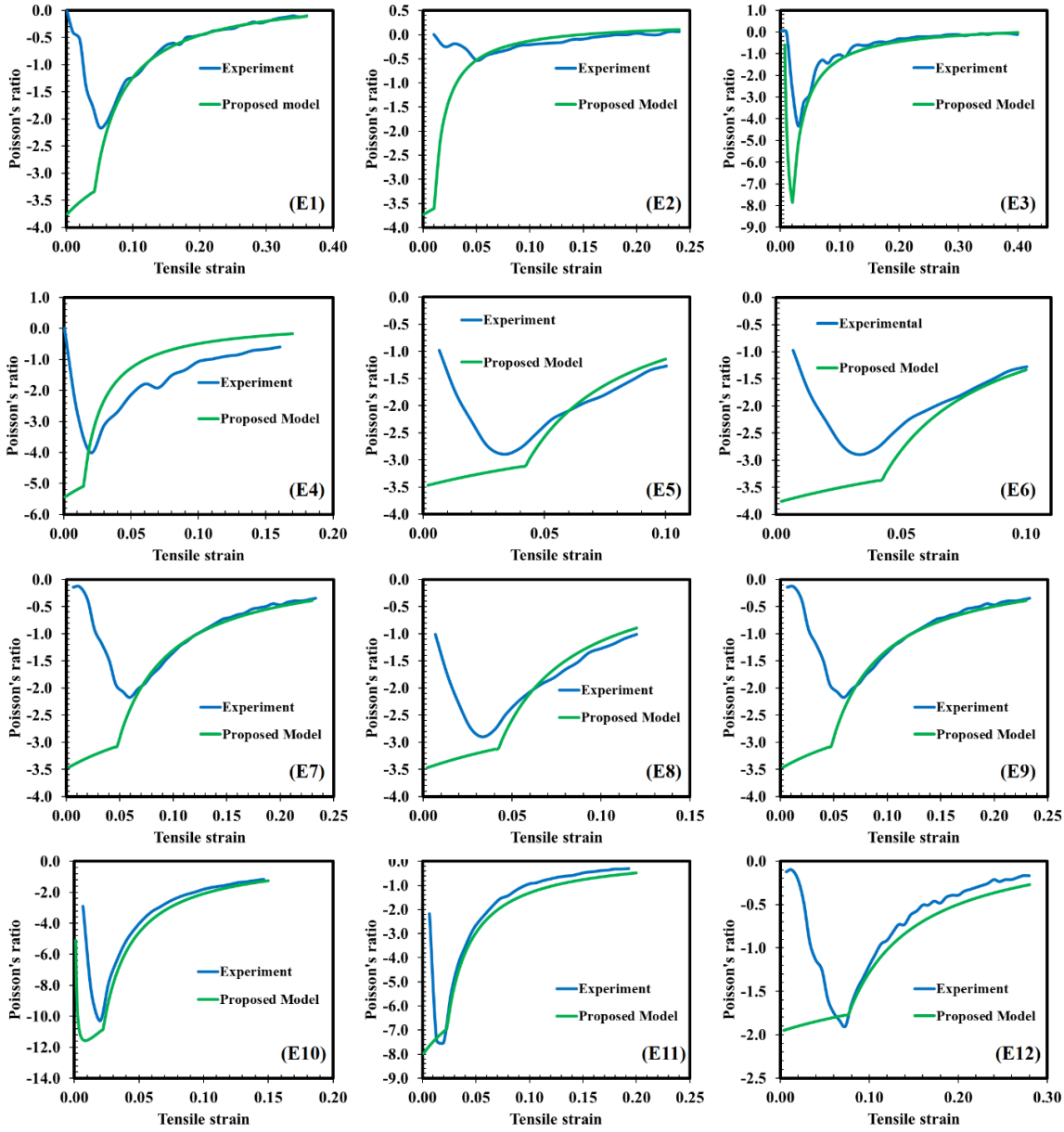

Fig. 6 Predicted Poisson's ratio-strain curves using the proposed model are based on previous experimental works cited from E1-E4 [18], E5 [19] E6 [26] E7-E12 [27]

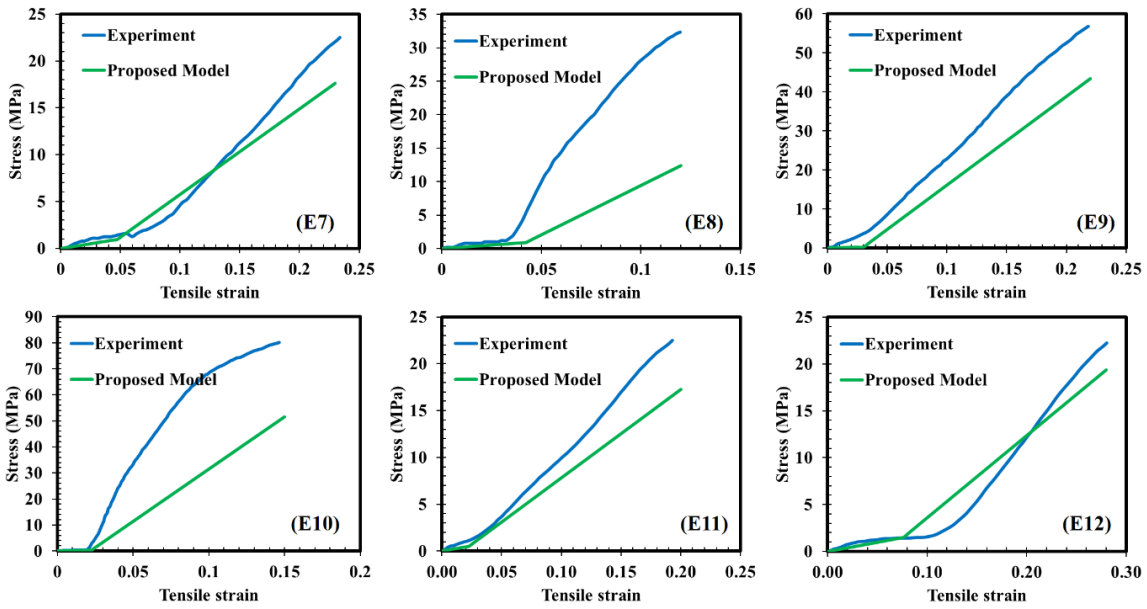

Fig. 7 Predicted stress-strain curves using the proposed model are based on previous experimental works cited from [27]

3-2 Theoretical disclosures

In the previous section, we demonstrated that the model effectively accounts for the structural impact on both the Poisson's ratio-strain and the stress-strain behaviors of A4PY. Consequently, this provides a theoretical foundation for conducting a parametric study with the developed model. Figure 6 illustrates how various structural parameters, such as the radius of soft yarn, Young's modulus of stiff yarn, and twist per meter of the structure, influence the Poisson's ratio-strain and stress-strain curves. It is evident that increasing the radius of the soft yarn and decreasing the twist per meter enhances Poisson's ratio of A4PY. However, alterations to the Young's modulus of the stiff yarn do not impact the Poisson's ratio, as shown in Figure 6a-c. In scenarios where the difference in Young's modulus between soft and stiff yarns is substantial (greater than 1000 times), the predictions correlate well with experimental values. Conversely, when the disparity in Young's modulus is less pronounced (less than 1000 times), discrepancies arise between experimental and predicted values. Practically speaking, a higher Young's modulus in the stiff yarn leads to a more negative Poisson's ratio in A4PY due to the stiff yarns displacing the soft yarns, promoting auxetic behavior.

When predicting the tensile behavior of A4PY using the developed model, it is observed that a smaller radius of soft yarn, a higher Young's modulus in stiff yarn, and a reduced twist per meter result in a higher Young's modulus of A4PY both before and after the jamming strain. This is because a smaller soft yarn radius or a reduced twist per meter increases the axial force along the structure, thereby enhancing A4PY's ability to withstand higher forces. Similarly, using stiffer yarn with a higher Young's modulus enhances this effect, particularly during the second stage of the tensile process, as shown in Figure 6d-f.

The developed model significantly enhances our understanding of the tensile behavior of A4PY by incorporating key structural parameters such as the radius of soft yarns, Young's modulus of stiff yarns, and twist per meter, enabling precise predictions of Poisson's ratio-strain and stress-strain relationships. This capability is vital for optimizing material design and functionality, particularly in applications requiring detailed mechanical response analysis under varied conditions. Furthermore, the model holds substantial potential for broader applications in composite and smart materials. It can guide the design of new composites with customized properties for industries such as aerospace and automotive and facilitate the creation of smart materials capable of adaptive responses to environmental stimuli. The predictive accuracy and adaptability of the model also make it a valuable tool in research and development, reducing the need for extensive physical testing by allowing researchers to simulate potential outcomes in advance. This model not only advances our understanding of A4PY but also opens avenues for innovative applications in both traditional and emerging material technologies, highlighting its importance in the development of high-performance materials.

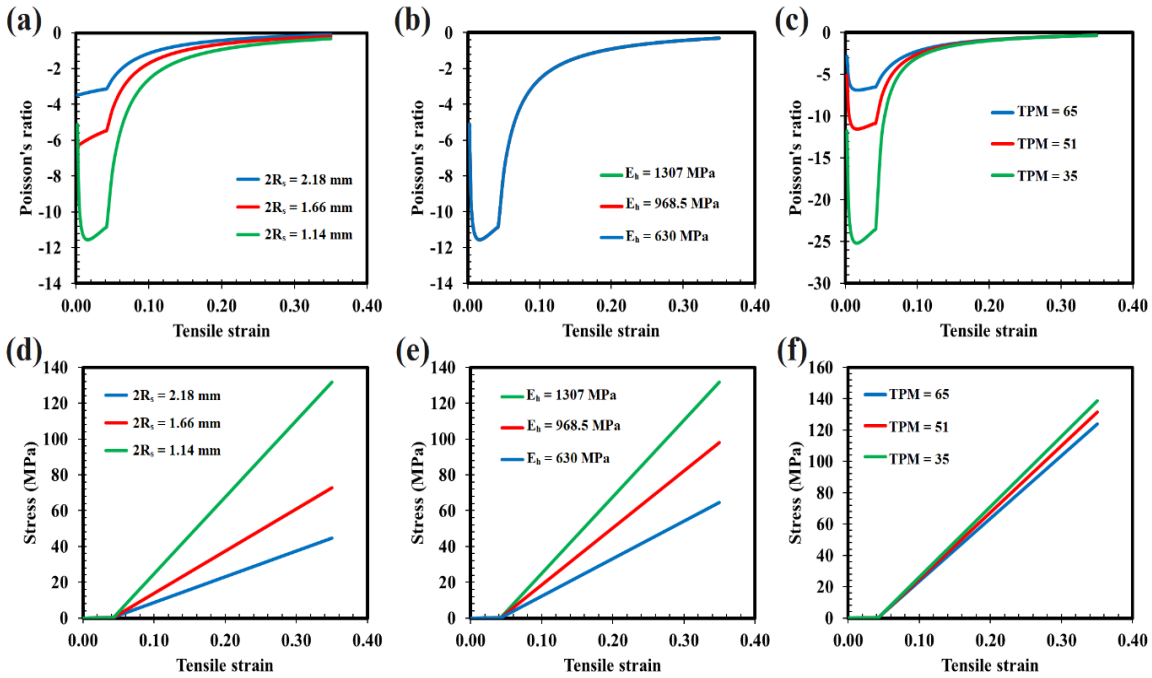

Fig. 8 Theoretical investigation of (a) effect of soft yarn radius (b) stiff yarn Young's modulus, and (d) twist per meter of structure on Poisson's ratio-strain curve, and (d) effect of soft yarn radius (e) Young's modulus, and (f) twist per meter of structure on stress-strain curve

4 CONCLUSIONS

This study presents analytical models developed to predict Poisson's ratio-strain and stress-strain behavior of A4PY. To validate these models, experimental data from prior studies are utilized. The key findings are summarized as follows:

- The proposed model for the Poisson's ratio-strain curve incorporates critical geometric parameters, including twisting angle, Poisson's ratio, and the radius of the components. However, the influence of mechanical properties, particularly the Young's modulus of the components, necessitates further refinement of the model to enhance its accuracy.
- The stress-strain curve model effectively accounts for geometric parameters such as twisting angle, Poisson's ratio, radius, and the Young's modulus of the components. Nevertheless, the model's precision in the plastic deformation region can be improved by replacing the assumption of linear tensile behavior with a nonlinear function that more accurately represents the material's response.

Overall, the proposed models are versatile tools, capable of predicting Poisson's ratio-strain and stress-strain behaviors for various applications. They offer potential as objective functions for optimizing the design of A4PY for targeted applications. Future work will focus on integrating these models with advanced methodologies, such as machine learning and deep learning, to enhance their predictive capabilities and broaden their applicability.

REFERENCES

[1] Z. Wang, C. Luan, G. Liao, J. Liu, X. Yao, and J. Fu, "Progress in auxetic mechanical metamaterials: structures, characteristics, manufacturing methods, and applications, *Advanced Engineering Materials*, vol. 22, no. 10, p. 2000312, 2020.

[2] P. U. Kelkar, H. S. Kim, K.-H. Cho, J. Y. Kwak, C.-Y. Kang, and H.-C. Song, "Cellular auxetic structures for mechanical metamaterials: A review, *Sensors*, vol. 20, no. 11, p. 3132, 2020.

[3] K. E. Evans, "Auxetic polymers: a new range of materials, *Endeavour*, vol.15, no.4, pp.170-174, 1991.

[4] G. Zhang, O. R. Ghita, C. Lin, and K. E. Evans, "Large-scale manufacturing of helical auxetic yarns using a novel semi-coextrusion process, *Textile research journal*, vol. 88, no. 22, pp.2590-2601, 2018.

[5] S. Liu, X. Pan, D. Zheng, Z. Du, G. Liu, and S. Yang, "Study on the structure formation and heat treatment of helical auxetic complex yarn, *Textile research journal*, vol. 89, no. 6, pp. 1003-1012, 2019.

[6] Z. Du, M. Zhou, H. Liu, and L. He, "Study on negative Poisson's ratio of auxetic yarn under tension: Part 1–Theoretical analysis, *Textile Research Journal*, vol. 85, no. 5, pp. 487-498, 2015.

[7] A. Sibal and A. Rawal, "Design strategy for auxetic dual helix yarn systems, *Materials Letters*, vol. 161, pp. 740-742, 2015.

[8] S. Liu, Z. Du, G. Liu, X. Pan, and T. Li, "Study on the tensile behavior of helical auxetic yarns by modeling and mechanical analysis, *The Journal of The Textile Institute*, vol. 112, no. 10, pp. 1531-1537, 2021.

[9] M. Razbin, M. Jamshidi Avanaki, A. A. A. Jeddi, and H. Dabiryan, "A systematic study on the predictability of different methods to predict the maximum Poisson's ratio of helical auxetic yarn, *The Journal of the Textile Institute*, vol. 113, no. 1, pp. 90-100, 2022.

[10] M. Kwietniewski and D. Miedzińska, "Numerical analysis of Helical Auxetic Yarn elastomeric core tension," in *AIP Conference Proceedings*, 2019, vol. 2078, no. 1: AIP Publishing.

[11] J. McAfee and N. H. Faisal, "Parametric sensitivity analysis to maximise auxetic effect of polymeric fibre based helical yarn, *Composite structures*, vol. 162, pp. 1-12, 2017.

[12] M. Razbin, M. Jamshidi Avanaki, A. A. Asghariyan Jeddi, and H. Dabiryan, "Maximum Negative Poisson's Ratio of Double-Core Helical Auxetic Yarns Under Uniaxial Loading: A Study on the Effect of Structural Parameters via Full Factorial Experimental Design Method, *Journal of Textiles and Polymers*, vol. 9, no. 3, pp. 37-44, 2021.

[13] G. Zhang, O. Ghita, and K. E. Evans, "The fabrication and mechanical properties of a novel 3-component auxetic structure for composites, *Composites Science and Technology*, vol. 117, pp. 257-267, 2015.

[14] Y. Shen and S. Adanur, "Mechanical analysis of the auxetic behavior of novel braided tubular structures by the finite element method, *Textile research journal*, vol. 89, no. 23-24, pp. 5187-5197, 2019.

[15] A. Lolaki, M. Zarrebini, D. Mostofinejad, M. Shanbeh, and S. M. Abtahi, "Intensification of auxetic effect in high stiffness auxetic yarns with potential application as the reinforcing element of composite, *Journal of Industrial Textiles*, vol. 51, no. 3_suppl, pp. 5169S-5185S, 2022.

[16] M. Razbin and R. Bagherzadeh, "Predicting the longitudinal young's modulus of helical auxetic yarn reinforced unidirectional composite, *The Journal of The Textile Institute*, vol. 114, no. 2, pp. 273-281, 2023.

[17] T. C. Lim, "Semi-auxetic yarns, *physica status solidi (b)*, vol. 251, no. 2, pp. 273-280, 2014.

[18] Z. Ge, H. Hu, and S. Liu, "A novel plied yarn structure with negative Poisson's ratio, *The Journal of the Textile Institute*, vol. 107, no. 5, pp. 578-588, 2016.
[19] J. Zeng and H. Hu, "A theoretical analysis of deformation behavior of auxetic plied yarn structure, *Smart Materials and Structures*, vol. 27, no. 7, p. 075003, 2018.
[20] N. Jiang and H. Hu, "Auxetic yarn made with circular braiding technology, *physica status solidi (b)*, vol. 256, no. 1, p. 1800168, 2019.
[21] M. Razbin, M. Jamshidi Avanaki, A. A. Asghariyan Jeddi, and H. Dabiryan, "Double-core helical auxetic yarn: a Novel structure, geometrical modeling and experimental verification, *The Journal of the Textile Institute*, vol. 113, no. 7, pp. 1256-1269, 2022.
[22] M. Razbin, M. J. Avanaki, and A. A. A. Jeddi, "Application of artificial neural network and full factorial method to predict the Poisson's ratio of double core helical auxetic yarn, *The Journal of the Textile Institute*, vol. 114, no. 2, pp. 198-206, 2023.
[23] L. Chen *et al.*, "Stretchable negative Poisson's ratio yarn for triboelectric nanogenerator for environmental energy harvesting and self-powered sensor, *Energy & Environmental Science*, vol. 14, no. 2, pp. 955-964, 2021.
[24] X. Guan, B. Xu, J. Huang, T. Jing, and Y. Gao, "Fiber-shaped stretchable triboelectric nanogenerator with a novel synergistic structure of opposite Poisson's ratios, *Chemical Engineering Journal*, vol. 427, p. 131698, 2022.
[25] R. Wu, S. Seo, L. Ma, J. Bae, and T. Kim, "Full-fiber auxetic-interlaced yarn sensor for sign-language translation glove assisted by artificial neural network, *Nano-Micro Letters*, vol. 14, no. 1, p. 139, 2022.
[26] J. Zeng, H. Cao, and H. Hu, "Finite element simulation of an auxetic plied yarn structure, *Textile research journal*, vol. 89, no. 16, pp.3394-3400, 2019.
[27] W. S. Ng and H. Hu, "Tensile and deformation behavior of auxetic plied yarns, *physica status solidi (b)*, vol. 254, no. 12, p. 1600790, 2017.